



OPEN ACCESS

EDITED BY

Ali Saleh Alshomrani,
King Abdulaziz University, Saudi Arabia

REVIEWED BY

Ahmed ElGendy,
The University of Texas at El Paso,
United States
S. D. Kaushik,
UGC-DAE Consortium for Scientific
Research Mumbai Centre, India

*CORRESPONDENCE

Akhtar Ali,
✉ akhtarhitec@gmail.com
Akif Safeen,
✉ akifsafeen@upr.edu.pk
Sayed M. Eldin,
✉ sayed.eldin22@fue.edu.eg

SPECIALTY SECTION

This article was submitted to Colloidal
Materials and Interfaces,
a section of the journal
Frontiers in Materials

RECEIVED 06 December 2022

ACCEPTED 16 January 2023

PUBLISHED 30 January 2023

CITATION

Ali A, Shah WH, Safeen A, Ali L, Tufail M,
Ullah Z, Safeen K, Eldin SM, R. Ali M,
Sohail M and Imran N (2023), Effect of Ca
doping on the arbitrary canting of
magnetic exchange interactions in
 $\text{La}_{1-x}\text{Ca}_x\text{MnO}_3$ nanoparticles.
Front. Mater. 10:1117793.
doi: 10.3389/fmats.2023.1117793

COPYRIGHT

© 2023 Ali, Shah, Safeen, Ali, Tufail, Ullah,
Safeen, Eldin, R. Ali, Sohail and Imran. This
is an open-access article distributed under
the terms of the [Creative Commons
Attribution License \(CC BY\)](https://creativecommons.org/licenses/by/4.0/). The use,
distribution or reproduction in other
forums is permitted, provided the original
author(s) and the copyright owner(s) are
credited and that the original publication in
this journal is cited, in accordance with
accepted academic practice. No use,
distribution or reproduction is permitted
which does not comply with these terms.

Effect of Ca doping on the arbitrary canting of magnetic exchange interactions in $\text{La}_{1-x}\text{Ca}_x\text{MnO}_3$ nanoparticles

Akhtar Ali^{1*}, Wiqar H. Shah¹, Akif Safeen^{2*}, Liaqat Ali¹,
Muhammad Tufail¹, Zakir Ullah¹, Kashif Safeen³, Sayed M. Eldin^{4*},
Mohamed R. Ali⁵, Muhammad Sohail⁶ and Naveed Imran⁷

¹Department of Physics, Faculty of Basic and Applied Sciences, International Islamic University, Islamabad, Pakistan, ²Department of Physics, University of Poonch Rawalakot, Rawalakot, Azad Jammu and Kashmir, Pakistan, ³Department of Physics, Abdul Wali Khan University Mardan, Mardan, Pakistan, ⁴Center of Research, Faculty of Engineering, Future University in Egypt, New Cairo, Egypt, ⁵Faculty of Engineering and Technology, Future University, New Cairo, Egypt, ⁶Department of Mathematics, Khwaja Fareed University of Engineering and Information Technology, Rahim Yar Khan, Pakistan, ⁷HITEC Schools and Colleges, HIT Taxila, Taxila, Pakistan

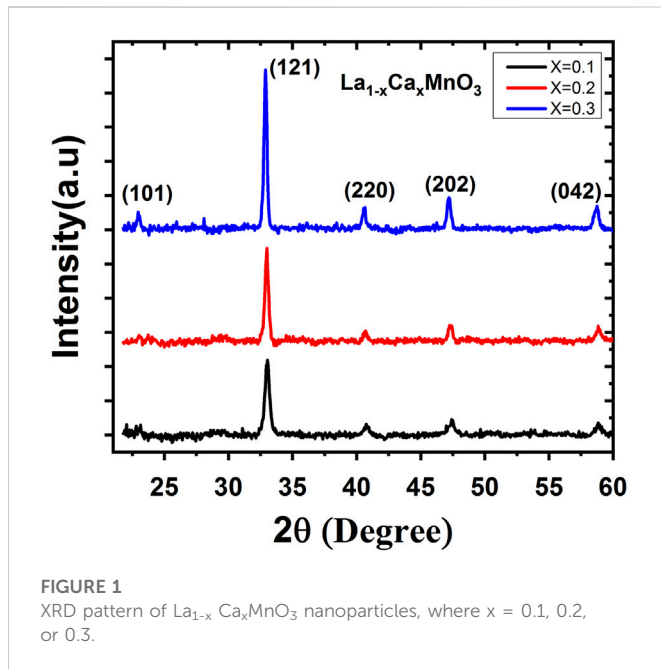
$\text{La}_{1-x}\text{Ca}_x\text{MnO}_3$ nanoparticles ($x = 0.1, 0.2, 0.3$) (LCMO NPs) were synthesized using the coprecipitation method. The prepared samples were investigated using x-ray diffraction (XRD), which confirmed the single-phase structure. The nanoparticle's crystallite size was determined using Debye–Scherrer's formula. Scanning electron microscopy showed that the size of the nanoparticles was between 33 nm and 55 nm. Energy-dispersive x-ray spectroscopy (EDX) was used to determine the elemental composition of samples. The four-probe method was used to measure the temperature-dependent electrical resistivity. Magnetic properties, such as hysteresis loop, magnetoresistance, and magnetization *versus* temperature, were measured using a vibrating sample magnetometer. The study of magnetization *versus* applied magnetic field $M(H)$ showed that, at 77 K, all the loops exhibit ferromagnetism. DC magnetization *versus* temperature at a 70-Oe-applied field for all samples showed a paramagnetic-ferromagnetic phase transition. A decrease in Curie temperature T_C after increasing the concentration of x was observed. The real and imaginary parts of temperature-dependent ac magnetic susceptibility were measured and revealed a transition from the ferromagnetic to the paramagnetic phase at a particular temperature T_C , with DC magnetization behavior.

KEYWORDS

nanomaterials, magnetic nanoparticles, Curie temperature, exchange interactions, magnetoresistance

1 Introduction

Hole-doped perovskite manganites $\text{R}_{1-x}\text{A}_x\text{MnO}_3$, where rare earth ion is indicated by R and divalent ions, such as Pb, Ca, Sr, or Ba, are represented by A, have drawn great technological and scientific interest for many decades. The potential properties that these materials can possess include a metal-insulator transition (T_{MI}) colossal magneto-resistance (CMR) effect, electronic phase transition, orbital ordering, charge ordering (T_{CO}), and a giant magnetic entropy effect (Dagotto et al., 2001; Gor'kov and Kresin, 2004; Mormooidae, 2009). The physical properties of $\text{La}_{1-x}\text{Ca}_x\text{MnO}_3$ synthesized by various methods have recently been studied. The structural, magneto-transport, and electrical properties of $\text{La}_{1-x}\text{Ca}_x\text{MnO}_3$ prepared using the sol-gel combustion method have been examined (Channagoudra et al., 2020). XRD for LCMO

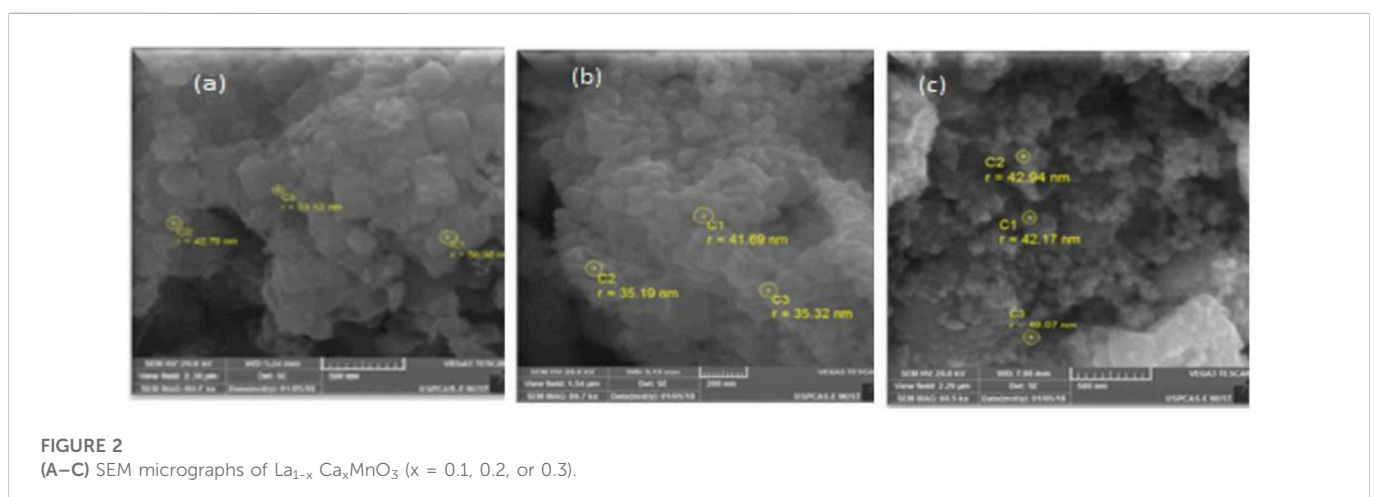


($x = 0.375$ and 0.625) confirmed the single-phase orthorhombic perovskite structure. The low magnetoresistance in $x = 0.625$ is observed due to charge order (CO). In the absence of a magnetic field, the metal-insulator (MI) was observed for sample $x = 0.375$ at 172 K. A significant decrease in resistivity was observed after the application of a magnetic field. Additionally, it has been shown that the size of the nanoparticles is directly dependent on the annealing temperature (Xia et al., 2017b). The LCMO samples were synthesized and annealed at 600°C, 650°C, and 700°C for 5 h in the absence of an applied magnetic field to study temperature-dependent resistivity. Metal-insulator transition at 266 K, 267 K, and 248 K was observed. Additionally, the same transitions have been found for two systems, LCMO-PAS (plasma activated sintering) and LCMO-HP (hot pressing), at a zero and 3T magnetic field at a temperature below 50 K; an upturn in resistivity shows an insulating behavior (Li et al., 2018b).

Temperature dependence on resistivity has also been reported for $\text{La}_{1-x}\text{Sr}_x\text{MnO}_3$ in the temperature range of 5–300 K with $x = 0.1, 0.2,$

and 0.3 at zero external magnetic field. An increase in T_p between $x = 0.1$ and $x = 0.3$ and a decrease in resistivity with increasing Sr concentration was observed (Van Cuong and Kim, 2009). The temperature dependence of ac susceptibility of LCMO and LCSMO showed a transition from a ferromagnetic to a paramagnetic state at 206 K and 277 K, respectively (Tank et al., 2015). Interesting results regarding ac susceptibility were obtained by a study of Fe-doped $\text{La}_{0.65}\text{Ca}_{0.35}\text{Mn}_{1-x}\text{Fe}_x\text{O}_3$ (Shah and Hasanain, 2010). Fe substitution gradually changed from a metallic ferromagnetic insulator to a ferromagnetic insulator at $T_c = 270\text{ K} - 79\text{ K}$. The increment in Fe concentration resulted in increased dissipation and disorder at low temperatures. The use of a DC field of 550 Oe resulted in a large decrease in susceptibility. The peaks of out-of-phase susceptibility broaden with increasing Fe concentration (Tola et al., 2017). M_s increases while H_c decreases with particle size. The larger H_c values at $D < 40\text{ nm}$ are caused by a magnetic dead layer. A broad phase transition has been shown for $D \leq 40\text{ nm}$, whereas transition is sharp for $D > 40\text{ nm}$. T_c increases initially then decreases slightly with increasing D above 40 nm (Xia et al., 2017b). This decrease in T_c with increasing annealing temperature or particle size is recognized as the decline of the double exchange interaction, as the bandwidth and mobility of the e_g electron decreases. This occurs because of the rise in Mn-O band length and the reduction in the Mn-O-Mn bond angle. A branching in the MFC (T) and MZFC (T) curve, showing a glass-like behavior, has been found for a wide range of temperatures. An M-H study showed that the values of M_s and M_r are greater for samples annealed at 650°C than those annealed at 600°C and 700°C.

The structural, magnetic, and electronic properties of these materials are strongly dependent on doping level. Therefore, in this study, we report on the effect of Ca doping on the transport and magnetic properties of $\text{La}_{1-x}\text{A}_x\text{MnO}_3$ nanoparticles with $x = 0.1, 0.2,$ or 0.3 . Different methods are used to synthesize these materials, such as a solid state reaction, the sol gel process, the molten salt route, and the glycerin-assisted combustion technique (Lu et al., 2007; Gubin, 2009; Prasad and Singh, 2011; Li et al., 2018a). However, these methods cause energy loss and environmental issues as they need expensive and toxic reagents and therefore cannot be used at a large scale (Gadani et al., 2017). In this study, we use the facile coprecipitation method, which has a simple operating procedure, is inexpensive, and can possibly create pure and homogeneous material that is environmental friendly.



2 Experimental techniques

LCMO nanoparticles were prepared using $\text{Mn}(\text{NO}_3)_2 \cdot 4\text{H}_2\text{O}$, $\text{CaCl}_2 \cdot 2\text{H}_2\text{O}$, and $\text{La}(\text{NO}_3)_3 \cdot 6\text{H}_2\text{O}$ as precursors purchased from Sigma-Aldrich with 99.99% purity. The desired stoichiometric amounts of these precursors were dissolved in deionized water, while NaOH was used as a precipitant. The first solution was continuously stirred at 80°C for 2 h to ensure homogeneity and the completion of the reaction. To maintain pH at 8.5, NaOH was added drop wise. The precipitate was filtered and cooled to room temperature. The powder was dispersed with ultrasonic waves in ethanol for 15 min to prepare mono-disperse LCMO nanoparticles and was then centrifuged and washed with distilled water. It was then dried in an oven for 1 h at 100°C . At 450°C , the dried samples were annealed in a furnace for 8 h. The same procedure was used for all samples.

We performed XRD (XPERT-3 Malvern Panalytical diffractometer system) using $\text{Cu K}\alpha$ radiation with a wavelength of 1.54 \AA over the angular range of $20^\circ \leq 2\theta \leq 70^\circ$ by step scanning results at a step size of 0.02 at a counting time of 3 s per step. Scanning electron microscopy (SEM-VEGA 3 TESKAN) was used to reveal the shape morphologies of all LCMO NPs. An EDX (SEM-VEGA 3 TESKAN) attached to the SEM was used to study the elemental composition and phase purity of the LCMO NPs. $M(H)$ behavior of $\text{La}_{1-x}\text{Ca}_x\text{MnO}_3$ ($x = 0.1, 0.2, 0.3$) was determined at a temperature of 77 K by applying a magnetic field at a strength of 10 kOe using a VSM. Magnetization *versus* temperature $M(T)$ was examined at a field of 70 Oe using field-cooled (FC) and zero-field-cooled (ZFC) protocols. A self-made ac probe with a commercial lock-in amplifier and split secondary (astatically wound) was used to study the ac susceptibility of all LCMO samples in the range $f = 573 \text{ Hz}$, $H_{ac} = 10 \text{ Oe}$, and $0 < H_{dc} < 550 \text{ Oe}$. A home-based solenoid magnet was used to orient the dc magnetic field in the same direction as the ac field. A commercial liquid nitrogen variable temperature cryostat was used to measure resistivity. We determined electrical resistance using air-drying conducting silver paste with the help of a standard four probe technique. A calibrated thermocouple Rh-Fe at a temperature range of 77 K–300 K was used to measure sample temperature. The accuracy of the temperature reading had a margin of error of 0.05 K. A digital voltmeter was used to determine voltage across the sample, and a constant current of 100 μA to 1 mA was provided.

3 Results and discussion

3.1 Structural analysis

The XRD patterns of the samples $\text{La}_{1-x}\text{Ca}_x\text{MnO}_3$ ($x = 0.1, 0.2, 0.3$) are shown in Figure 1. After fitting to the space group Pbnm and JCPDS No 89-0662, all the peaks matched the standard orthorhombic structure of perovskite manganite nanoparticles [6]. At diffraction angles $2\theta = 22.50^\circ, 32.85^\circ, 40.45^\circ, 48.30^\circ$, and 58.75° , the peaks were indexed to (101), (121), (220), (202), and (042) planes. No additional and unidentified peaks were found, revealing that impurities were not present in the samples. It shows that the system is structurally single phase. The range of crystallite sizes was 25–32 nm using Debye–Scherrer's formula ($D = 0.9\lambda/\beta\cos\theta$) (Safeen et al., 2022a; Safeen et al., 2022b), where “D” represents the crystallite size, “ λ ” is the wavelength of the x-ray, “ θ ” is the Bragg

diffraction angle, and “ β ” is the full width at the half maximum (FWHM) of the diffraction peak (Asghar et al., 2020).

3.2 Morphological studies

SEM images for $\text{La}_{1-x}\text{Ca}_x\text{MnO}_3$ ($x = 0.1, 0.2, \text{ or } 0.3$) are featured in Figures 2A–C, which shows agglomerative particles that were, on average, 33–46 nm in size with a cage-like surface morphology. The samples were bulky and porous as gas was released in large amounts during heat treatment and sonication. The samples overall have a sphere-shaped cage-surface morphology.

3.3 Energy dispersive X-ray (EDX) spectroscopy

EDX spectra for $\text{La}_{1-x}\text{Ca}_x\text{MnO}_3$ ($x = 0.1, 0.2, \text{ or } 0.3$) is shown in Figures 3A–C, which shows the presence of La, Mn, O, and Ca peaks, confirming elemental compositional and phase purity. No extra peaks related to impurities can be observed. The atomic percentage of La, Ca, Mn, and O obtained from EDX spectra are in close agreement with the initial values used during synthesis. Elemental percentages of samples are shown in Table 1.

3.4 $M(H)$ loops

The field-dependent magnetization $M(H)$ behavior of $\text{La}_{1-x}\text{Ca}_x\text{MnO}_3$ ($x = 0.1, 0.2, \text{ and } 0.3$) at 77 K is shown in Figure 4, which shows that coercivity increases from $x = 0.1$ to $x = 0.3$. All the $M(H)$ loops showed ferromagnetic behavior, as confirmed by the $M(T)$ study. The enhanced coercivity could be attributed to single domain to multidomain magnetic behavior and randomly oriented equiaxial cubic magneto-crystalline anisotropy due to larger grain size (Chinnasamy et al., 2003). Additionally, the saturation magnetization increased with the concentration of x due to random canting of the grain surface spin occurring from the competition between ferromagnetic (FM) and anti-ferromagnetic (AFM) exchange interactions close to the surface. The M_r/M_s ratio was initially constant but decreased with doping concentration. Atoms have several domains of huge size, so magnetization reversal is gained by domain wall motion, thus coercivity is small. Magnetization reversal remains uniform for the single domain. For instance, it is necessary to respond with this field when the size of the spherical particle is larger for the identical spin rotation. Hence, initially, the energy wall for magnetization rotation increases with increasing particle size within a range of particle sizes. Therefore, coercivity increases because of the increase in particle size (Chinnasamy et al., 2003; Shah et al., 2012). The values of different parameters, such as M_s , M_r/M_s , M_r and H_c , obtained from the magnetic measurement of the synthesized nanoparticles are shown in Table 2.

3.5 Temperature-dependent DC magnetization

The temperature-dependent magnetization $M(T)$ for three samples at a magnetic field of 70 Oe is shown in Figure 5.

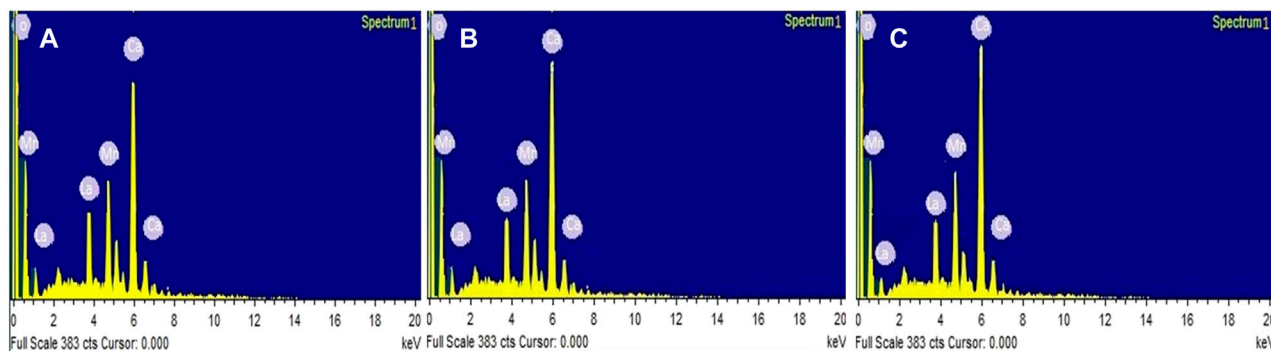


FIGURE 3 (A–C) EDX spectra of $\text{La}_{1-x}\text{Ca}_x\text{MnO}_3$ ($x = 0.1, 0.2,$ or 0.3).

TABLE 1 Elemental composition of $\text{La}_{1-x}\text{Ca}_x\text{MnO}_3$ ($x = 0.1, 0.2,$ and 0.3).

Samples	O (%)	La (%)	Ca (%)	Mn (%)	Total
$\text{La}_{0.9}\text{Ca}_{0.1}\text{MnO}_3$	47.41	35.61	13.64	3.34	100
$\text{La}_{0.8}\text{Ca}_{0.2}\text{MnO}_3$	46.32	33.55	16.53	3.60	100
$\text{La}_{0.7}\text{Ca}_{0.3}\text{MnO}_3$	43.34	32.45	20.15	4.06	100

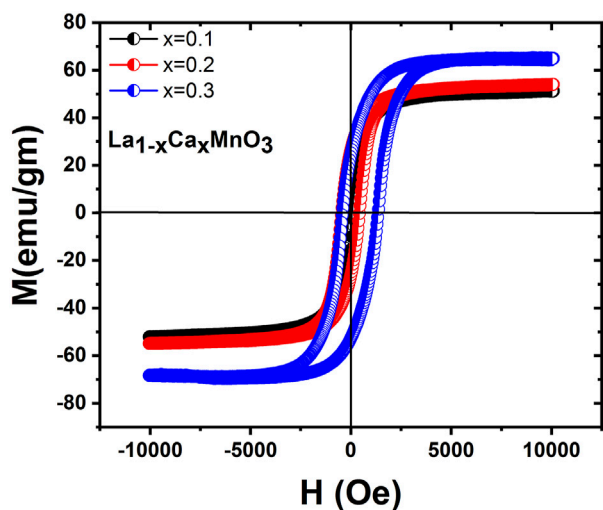


FIGURE 4 Field dependence of magnetization for $\text{La}_{1-x}\text{Ca}_x\text{MnO}_3$ samples at Ca concentrations of $x = 0.1, 0.2,$ and 0.3 .

TABLE 2 Saturation-magnetization (M_s), remanent/saturation-magnetization (M_r/M_s), remanent magnetization (M_r), and coercive-field (H_c) of $\text{La}_{1-x}\text{Ca}_x\text{MnO}_3$ ($x = 0.1, 0.2,$ and 0.3).

Samples	M_s (emu/gm)	M_r/M_s	M_r (emu/gm)	H_c (Oe)
$\text{La}_{0.9}\text{Ca}_{0.1}\text{MnO}_3$	51.55	0.28	14.34	79.53
$\text{La}_{0.8}\text{Ca}_{0.2}\text{MnO}_3$	54.28	0.287	15.57	208.9
$\text{La}_{0.7}\text{Ca}_{0.3}\text{MnO}_3$	66.50	0.195	12.97	172.58

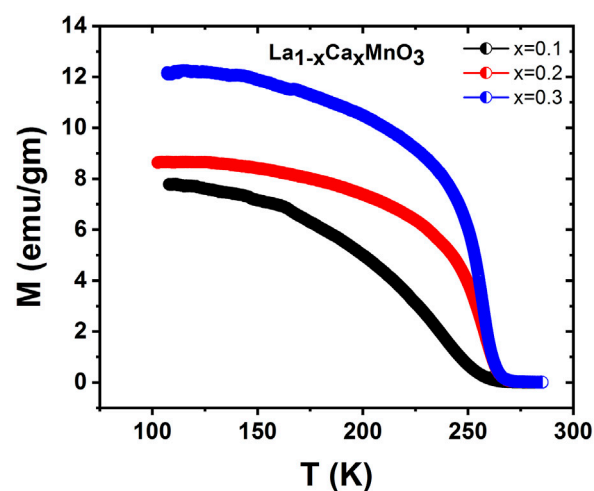
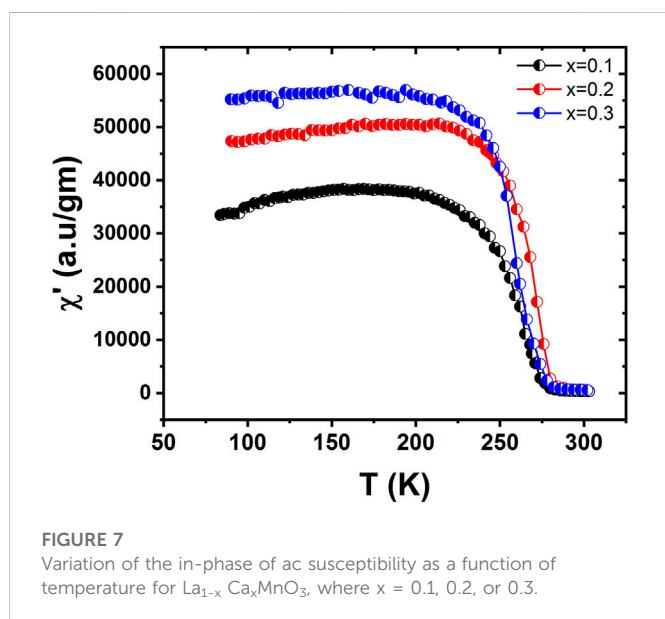
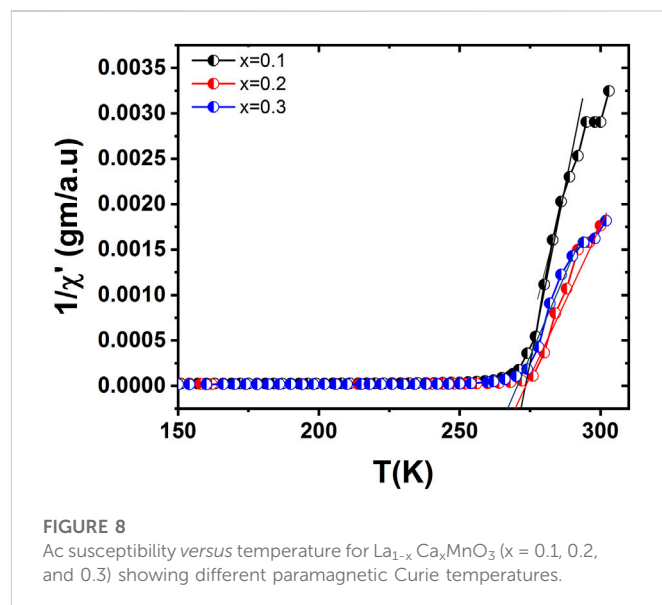
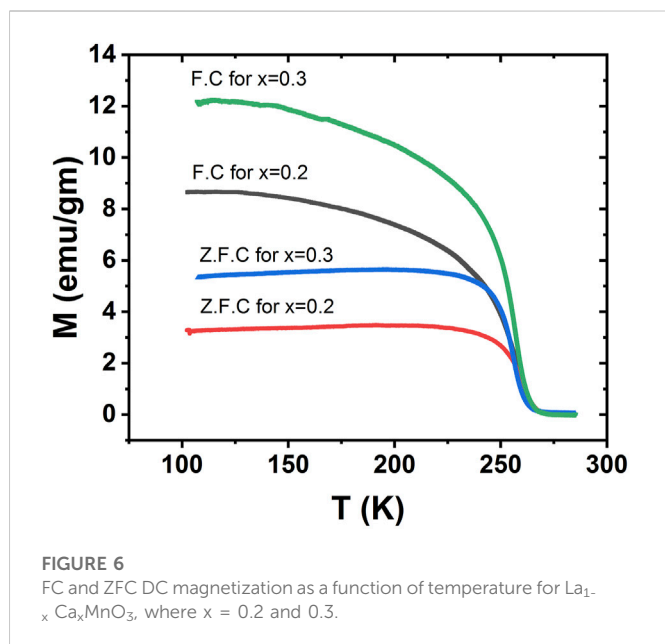


FIGURE 5 Magnetization as a function of temperature for $\text{La}_{1-x}\text{Ca}_x\text{MnO}_3$ ($x = 0.1, 0.2,$ and 0.3).

Paramagnetic (PM) to ferromagnetic (FM) transition was observed due to cooling at a particular temperature of the material. The Curie temperatures T_c (the temperature representing the peak of $-dM/dT$ in the M vs T curve) were 258 K, 255 K, and 250 K for $x = 0.1, 0.2,$ and 0.3 , respectively. The fall in T_c was caused by a decline in double exchange due to a reduction in mobility electrons and bandwidth. This reduction is up on rise in bond-length and decline in bond-angle of Mn-O-Mn (Shah, 2011).

Examination of $M(T)$ behavior of $\text{La}_{1-x}\text{Ca}_x\text{MnO}_3$ ($x = 0.2$ and 0.3) at a field of 70 Oe for FC and ZFC conditions to determine the behavior of magnetic spin freezing is shown in Figure 6. A split in the magnetization field cooled *versus* temperature and magnetization zero field cooled *versus* temperature curves over a wide temperature range. Upon cooling, the magnetic moment increased for all samples up to the lowest temperature for FC curves. A phase transition from paramagnetic to ferromagnetic was observed, but ZFC was different from FC, in which magnetic moments decreased as the temperature fell. We observed a huge difference in magnetization at lower temperatures between FC and ZFC curves. The dissimilarity between ZFC and FC magnetization was due to the significant spin



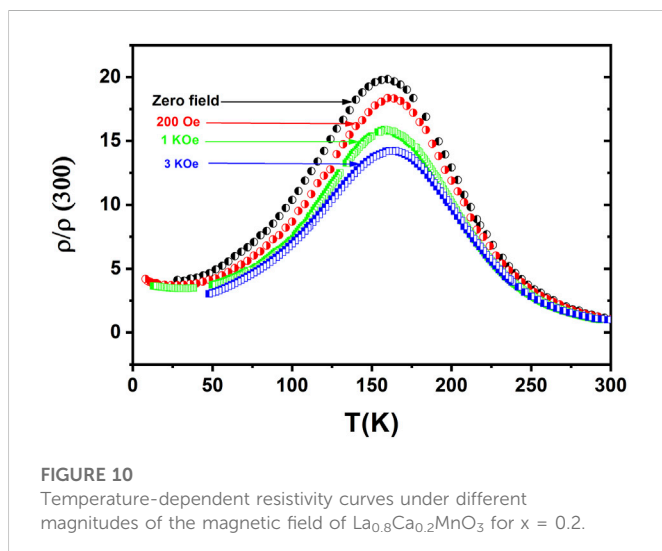
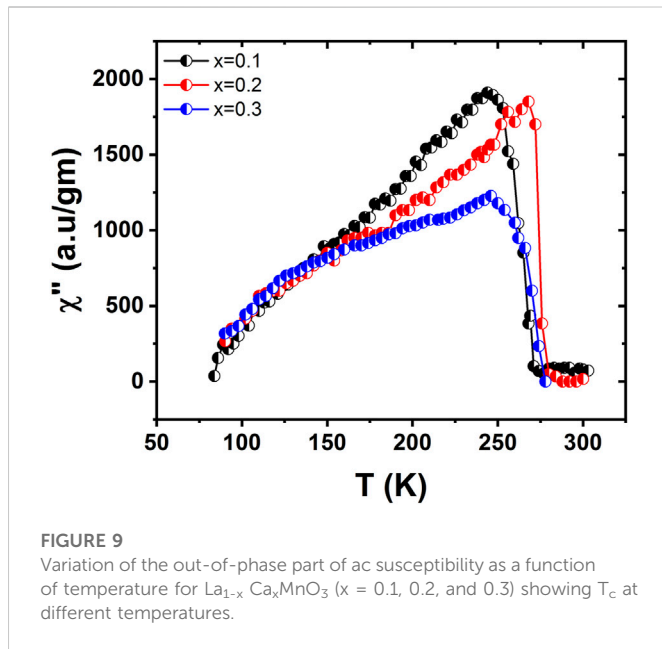
disorder and competing interaction between different phases (Hasanain et al., 2004). For FC curves, the maximum values of magnetization were 8.47 emu/gm and 12.16 emu/gm for $x = 0.2$ and 0.3 , respectively, while for ZFC curves, these values were 3.49 emu/gm and 5.49 emu/gm, respectively. As the temperature increased this difference minimized, and finally both curves merged. Such a behavior can be explained by the fact that when temperature is low the magnetic moment becomes frozen so that there is no order state in the long range. As a result of this spin disorder, strong competition occurred among ferromagnetic double-exchange (DE) and anti-ferromagnetic super-exchange (SE) so that a specific spin could obtain contradictory information, such as how to align with its neighbors due to exchange energy (Xia et al., 2017a). It may not be feasible to choose an assured spin configuration for the system to be

able to minimize its energy. This decrease of the magnetic moment is due to frustration. Between 240 K and 258 K, there is a delay in the increase in the magnetic moment during transition. The super exchange and strong double exchange magnetic interaction between Mn^{4+} and Mn^{3+} ions reduces the increase due to low temperature. As a result, there is competition between two phases and a spin-glass-like phase occurs due to the generation of some degree of frustration resulting from such a FM and AFM interaction. When the metallic-like conduct disappears, distinctive glass-like behavior is observed with small ions (Shah, 2011).

3.6 ac susceptibility measurement

There are two phases in which ac susceptibility measurements of the samples can be taken, namely, the in-phase and out-of-phase behavior as a function of temperature. Figure 7 shows the in-phase part of ac susceptibility. A sharp increase was observed at approximately 275 K, peaking at approximately 250 K. After the peak, there was a steady fall of ferromagnetic ac susceptibilities, with a sharp decline starting at approximately 100 K. A phase transition from the paramagnetic to the ferromagnetic phase occurred for all the samples in the transition region. Figure 7 shows that as Ca content increases, susceptibilities and sharpness in the transition region systematically decrease. Additionally, a decrease from the peak to the smallest value was observed. An increase of Ca concentration results in dissipation and spin disorder at low temperatures (Shah and Safeen, 2012). The presence of Ca results in a distortion not found in the XRD pattern. There is a possibility that an AFM arrangement is favored by local distortion catalyzed by Ca ions. Ferromagnetic clusters are found in the paramagnetic phase region. These ferromagnetic clusters increase in volume so that there is a complete ferromagnetic transition. However, in the clustering region, a continuous fluctuation occurs at high temperatures (Shah and Hasanain, 2010).

The behavior of the imaginary part of ac susceptibility is quite dissimilar from the real part as it sharply decreases at high T_c . The values of T_c for three samples ($x = 0.1, 0.2,$ and 0.3) were 272.01 K,



271.20 K, and 265.87 K, respectively, as shown in Figure 8. The out-of-phase part of susceptibility occurs because of spin direction and/or fluctuation losses. At phase transition, these losses become large. Within the low temperature region, the generation of losses is dependent on the merger of small clusters to form the major clusters. The fluctuation in the magnetization is proportional to the loss components for a system that is going through a magnetic transition, as described by the fluctuation dissipation theorem (Karoblis et al., 2020). The dynamical changes occurring in the critical region are related to the lost components. The development of dynamical correlation of the spin occurs due to energy losses that appear in the behavior. The variation of the out-of-phase part of ac susceptibility is shown in Figure 9. The peaks in the out-of-phase part of susceptibility occur near the T_c , where $M(T)$ shows no specific

structure except for the decrease of the variations in magnetization. The losses continue growing to a point at which the magnetization starts to rise sharply. This occurs during the persistent fast growth of small clusters in this range. These small clusters decrease in number at lower temperatures (Supplementary Material S1).

3.7 Resistivity measurements

To study the thermal fluctuation mechanism, the four-probe method was employed to determine the temperature-dependent electrical resistivity of $\text{La}_{0.8}\text{Ca}_{0.2}\text{MnO}_3$ nanoparticles. Figure 10 shows the effect of the applied magnetic field on resistivity in different temperature ranges. The values of resistivity were $1.4 \Omega\text{-cm}$ with the cooling protocol and $1.5 \Omega\text{-cm}$ with heating. This result shows that the transition temperature for the cooling curve rose as the magnetic field increased from 0 to 3 KOe. Additionally, resistivity decreased upon application of the magnetic field, as the microstructure of the large-range grain domain was parallel to the applied field. When the magnetic field was increased, the large-range magnetic array was increased, resulting in a decrease in resistivity. A rapid change in metal-to-insulator transition peak temperature (T_p) was observed. At room temperature, the sample was a semiconductor and had a temperature above the peak, i.e., at $T_p = 170 \text{ K}$ it exhibited metallic behavior. This alteration is related to magnetic ordering. The double-exchange mechanism defines the co-occurrence of FM and metallic behavior. At the highest value of Hund's exchange energy, the conductivity maximizes. Thus, ferromagnetism is associated with metal-like behavior. T_p is rather different for heating and cooling curves (Hao et al., 2013). T_p is low compared to normal. This drop of T_p is caused by the decrease of oxygen (Van Cuong and Kim, 2009). Identical and smaller particles have unlike stoichiometric oxygen. The deduction of oxygen reduces Mn^{4+} to Mn^{3+} . It preserves the electrical neutrality of the assemblage. The elimination of the oxygen bond stops the conduction pathways for e_g electrons. For the large range, the insulating part is further enhanced in the high-temperature range. With the rise in temperature, these defects decrease resistivity, resulting in an insulating appearance.

4 Conclusion

In conclusion, coprecipitation is a facile method for preparing LCMO nanoparticles. The XRD results show that prepared samples are pure in phase, and doping has no effect on the space group Pbnm. Particle size, identified by SEM, confirmed the nanocrystalline structure of the LCMO system. The hysteresis study revealed an increase in saturation magnetization with the increase of Ca because of arbitrary canting of the grain surface spin occurring near the surface of the competition between FM and AFM exchange interactions. A bifurcation in the magnetization FC and magnetization ZFC versus temperature curves over a wide range of temperatures was observed. The addition of Ca increased spin disorder, resulting in a decrease in the in-phase part of susceptibilities. The out-of-phase part of susceptibility occurred

due to the losses that were proportional to the fluctuation in the magnetization of a system. Resistivity measurements showed that the sample is a semiconductor at room temperature and becomes metallic above the peak transition temperature. Additionally, resistivity decreased as a function of the applied field. The investigated system may be used in magnetoresistance and other related applications.

Data availability statement

The raw data supporting the conclusion of this article will be made available by the authors, without undue reservation.

Author contributions

Conceptualization (AA, WS, and AS); Formal analysis (KS, MT, ZU, LA, SE, and NI); Investigation (MS, MR, and AA); Methodology (AA and WS); Project administration (WS); Supervision (WS); Writing—original draft (AA, WS, SE, and NI); Writing—review and editing (SE, AA, WS, KS, MT, ZU, LA, and AS).

References

- Asghar, G., Asri, S., Khuro, S. N., Tariq, G. H., Awan, M., Irshad, M., et al. (2020). Enhanced magnetic properties of barium hexaferrite. *J. Elec Materi* 49, 4318–4323. doi:10.1007/s11664-020-08125-7
- Channagoudra, G., Saw, A. K., and Dayal, V. (2020). Low temperature spin polarized tunnelling magneto-resistance in La_{1-x}CaxMnO₃ (x=0.375 and 0.625) nanoparticles. *Emergent Mat.* 3, 45–49. doi:10.1007/s42247-019-00067-z
- Chinnasamy, C., Jeyadevan, B., Shinoda, K., Tohji, K., Djayaprawira, D., Takahashi, M., et al. (2003). Unusually high coercivity and critical single-domain size of nearly monodispersed CoFe₂O₄ nanoparticles. *Appl. Phys. Lett.* 83, 2862–2864. doi:10.1063/1.1616655
- Cuong, P., and Kim, D. H. (2009). Effect of strontium doping level on electrical transport and magnetic properties of La_{1-x}SrxMnO₃ perovskite nanoparticles. *J. Phys. Conf. Ser.* 187, 012090. doi:10.1088/1742-6596/187/1/012090
- Dagotto, E., Hotta, T., and Moreo, A. (2001). Colossal magnetoresistant materials: The key role of phase separation. *Phys. Rep.* 344, 1–153. doi:10.1016/s0370-1573(00)00121-6
- Gadani, K., Keshvani, M., Dhruv, D., Boricha, H., Rathod, K., Prajapati, P., et al. (2017). Low field magnetoelectric and magnetotransport properties of sol-gel grown nanostructured LaMnO₃ manganites. *J. Alloys Compd.* 719, 47–57. doi:10.1016/j.jallcom.2017.05.165
- Gor'kov, L. P., and Kresin, V. Z. (2004). Mixed-valence manganites: Fundamentals and main properties. *Phys. Rep.* 400, 149–208. doi:10.1016/j.physrep.2004.08.003
- Gubin, S. P. (2009). *Magnetic nanoparticles*. John Wiley & Sons.
- Hao, F., Jing, D., Xiao-Peng, H., Fang-Yi, C., and Jun, C. (2013). Sol-gel synthesis of perovskite La_{1-x}CaxMnO₃ (x=0 similar to 0.4) nanoparticles for electrocatalytic oxygen reduction. *Chin. J. Inorg. Chem.* 29, 1617–1625.
- Hasanain, S., Shah, W. H., Mumtaz, A., Nadeem, M., and Akhtar, M. (2004). Re-entrant spin freezing behavior in La_{0.85}Ca_{0.15}Mn_{0.95}Fe_{0.05}O₃ manganite. *J. magnetism magnetic Mater.* 271, 79–87. doi:10.1016/j.jmmm.2003.09.020
- Karoblis, D., Mazeika, K., Baltrunas, D., Lukowiak, A., Strek, W., Zarkov, A., et al. (2020). Novel synthetic approach to the preparation of single-phase BixLa_{1-x}MnO_{3+δ} solid solutions. *J. Sol-Gel Sci. Technol.* 93, 650–656. doi:10.1007/s10971-019-05098-w
- Li, S., Wang, C., Liu, H., Li, L., Shen, Q., Hu, M., et al. (2018a). Effect of sintering temperature on structural, magnetic and electrical transport properties of La_{0.67}Ca_{0.33}MnO₃ ceramics prepared by Plasma Activated Sintering. *Mater. Res. Bull.* 99, 73–78. doi:10.1016/j.materresbull.2017.10.049
- Li, S., Wang, C., Zhou, D., Liu, H., Li, L., Shen, Q., et al. (2018b). Preparation of dense La_{0.67}Ca_{0.33}MnO₃ ceramics by plasma activated sintering and hot-pressing. *Ceram. Int.* 44, 550–555. doi:10.1016/j.ceramint.2017.09.210
- Lu, A. H., Salabas, E. E. L., and Schüth, F. (2007). Magnetic nanoparticles: Synthesis, protection, functionalization, and application. *Angew. Chem. Int. Ed.* 46, 1222–1244. doi:10.1002/anie.200602866
- Mormoopidae (2009). “Leaf-nosed bat,” in *Encyclopædia britannica* (Britannica).
- Prasad, R., and Singh, P. (2011). Applications and preparation methods of copper chromite catalysts: A review. *Bull. Chem. React. Eng. Catal.* 6, 63–113. doi:10.9767/bcrec.6.2.829.63-113
- Safeen, A., Safeen, K., Shafique, M., Iqbal, Y., Ahmed, N., Rauf Khan, M. a. R., et al. (2022a). The effect of Mn and Co dual-doping on the structural, optical, dielectric and magnetic properties of ZnO nanostructures. *RSC Adv.* 12, 11923–11932. doi:10.1039/d2ra01798a
- Safeen, A., Safeen, K., Ullah, R., ZulfqarShah, W. H., Shah, Q., Zaman, K., et al. (2022b). Enhancing the physical properties and photocatalytic activity of TiO₂ nanoparticles via cobalt doping. *RSC Adv.* 12, 15767–15774. doi:10.1039/d2ra01948e
- Shah, W. H. (2011). Dynamic response in Fe-doped La_{0.65}Ca_{0.35}Mn_{1-x}Fe_xO₃: Rare-Earth manganites. *J. Mat. Res.* 26, 2599–2603. doi:10.1557/jmr.2011.228
- Shah, W. H., and Hasanain, S. (2010). Ac susceptibility studies in Fe doped La_{0.65}Ca_{0.35}Mn_{1-x}Fe_xO₃: Rare Earth manganites. *J. Appl. Phys.* 108, 113907. doi:10.1063/1.3517113
- Shah, W. H., and Safeen, A. (2012). Effects of frequency on AC conductivity and magnetoresistance in doped La_{0.65}Ca_{0.35}MnO₃ manganites. *J. Elec Materi* 41, 2243–2249. doi:10.1007/s11664-012-2092-8
- Shah, W. H., Safeen, K., and Rehman, G. (2012). Effects of divalent alkaline Earth ions on the magnetic and transport features of La_{0.65}A_{0.35}Mn_{0.95}Fe_{0.05}O₃ (A = Ca, Sr, Pb, Ba) compounds. *Curr. Appl. Phys.* 12, 742–747. doi:10.1016/j.cjap.2011.10.015
- Tank, T. M., Bodhaye, A., Mukovskii, Y. M., and Sanyal, S. (2015). “Electrical-transport, magnetoresistance and magnetic properties of La_{0.7}Ca_{0.3}MnO₃ and La_{0.7}Ca_{0.24}Sr_{0.06}MnO₃ single crystals,” in *AIP conference proceedings* (AIP Publishing LLC), 100027.
- Tola, P., Kim, H., Kim, D., Phan, T., Rhyee, J., Shon, W., et al. (2017). Tunable magnetic properties and magnetocaloric effect of off-stoichiometric LaMnO₃ nanoparticles. *J. Phys. Chem. Solids* 111, 219–228. doi:10.1016/j.jpcc.2017.07.022
- Xia, W., Li, L., Wu, H., Xue, P., and Zhu, X. (2017a). Molten salt route of La_{1-x}Ca_xMnO₃ nanoparticles: Microstructural characterization, magnetic and electrical transport properties. *Mater. Charact.* 131, 128–134. doi:10.1016/j.matchar.2017.07.002
- Xia, W., Li, L., Wu, H., Xue, P., and Zhu, X. (2017b). Structural, morphological, and magnetic properties of sol-gel derived La_{0.7}Ca_{0.3}MnO₃ manganite nanoparticles. *Ceram. Int.* 43, 3274–3283. doi:10.1016/j.ceramint.2016.11.160

Conflict of interest

NI was employed by the company Heavy Industries Taxila.

The remaining authors declare that the research was conducted in the absence of any commercial or financial relationships that could be construed as a potential conflict of interest.

Publisher's note

All claims expressed in this article are solely those of the authors and do not necessarily represent those of their affiliated organizations, or those of the publisher, the editors and the reviewers. Any product that may be evaluated in this article, or claim that may be made by its manufacturer, is not guaranteed or endorsed by the publisher.

Supplementary material

The Supplementary Material for this article can be found online at: <https://www.frontiersin.org/articles/10.3389/fmats.2023.1117793/full#supplementary-material>